Quarkonium at non-zero isospin density

William Detmold,[1] Stefan Meinel,[1] and Zhifeng Shi[2, 3]

[1]*Center for Theoretical Physics, Massachusetts Institute of Technology, Cambridge, MA 02139, USA*
[2]*Department of Physics, The College of William & Mary, Williamsburg, VA 23187, USA*
[3]*Jefferson Lab, Newport News, VA 23606, USA*

We calculate the energies of quarkonium bound states in the presence of a medium of nonzero isospin density using lattice QCD. The medium, created using a canonical (fixed isospin charge) approach, induces a reduction of the quarkonium energies. As the isospin density increases, the energy shifts first increase linearly and then saturate at an isospin density where a qualitative change in the behaviour of the energy density of the medium has been previously observed. This provides further support to the conjecture that the medium undergoes a transition from a pion gas to a Bose-Einstein condensed phase at this point. The reduction of the quarkonium energies becomes more pronounced as the heavy-quark mass is decreased, similar to the behaviour seen in two-colour QCD at non-zero quark chemical potential. In the process of our analysis, the Υ–π and η_b–π scattering phase shifts are determined at low momentum and found to be small.

I. INTRODUCTION

An important probe of exotic phases of QCD matter is the way in which heavy quarkonium propagation is modified by by the presence of that matter. The heavy quarks can in some sense be viewed as separable from the medium which is predominantly composed of light quark and gluonic degrees of freedom. At non-zero temperature, the suppression of the propagation of J/ψ particles is a key signature for the formation of a quark-gluon plasma [1]. This suppression has been observed for charmonium in various experiments at SPS, RHIC and the LHC and recently in the Υ spectrum at the LHC [2]. Quarkonium propagation is naturally also expected to be a sensitive probe of other changes of phase such as those that occur at high density or large isospin density.

Since the effects of QCD matter on quarkonia are essentially non-perturbative in origin, a systematic evaluation requires input from lattice QCD. At some level, these effects can be distilled to a change in the potential between the quark–anti-quark ($Q\overline{Q}$) pair that binds them into quarkonium. At non-zero temperature but zero density, this has been studied extensively using lattice QCD (see Ref. [3] for a recent overview) where strong screening effects are seen near the deconfinement scale. Significant effects are also seen in investigations of the properties of charmonium and bottomonium spectral functions at non-zero temperature (see [3, 4]).

Modifications of the potential or quarkonium properties will also occur for non-zero density. Ref. [5] has investigated the static potential in the presence of a gas of pions and below we briefly address how the medium affects the binding of quarkonium through solving the Schrödingier equation for the modified potential. As the main focus of this work, however, we explore the effects of isospin charge density on quarkonium bound state energies more directly by using lattice NRQCD (non-relativistic QCD) to compute quarkonium correlation functions in the presence of a medium of varying isospin chemical potential. At low isospin densities, and

correspondingly low chemical potentials, we find that the ground state energy of the quarkonium systems decreases with increasing density, showing qualitative agreement between the potential model calculation and the QCD calculation. However, at an effective isospin chemical potential $\mu_I \sim \mu_{I,\text{peak}} = 1.3\ m_\pi$ (where previous calculations of the energy density of the isospin medium have suggested a transition to a Bose-Einstein condensed state [6] in line with theoretical expectations [7]), the effect of the medium on the quarkonium energy saturates to a constant shift. At still larger chemical potentials, the determination of the energy shift becomes statistically noisy. The marked change in behaviour provides additional support to the notion of the change in phase of the system.

Our study is presented as follows. In Section II, we construct an isospin density dependent potential model of quarkonium states, and calculate the expected shift of the quarkonium energies in the medium. Section III presents the methodology of the lattice QCD calculation of these energy shifts, with results presented in Sections IV and V. We conclude with a discussion of the results and possible extensions to the current work.

II. MODIFICATION OF THE STATIC QUARK–ANTI-QUARK POTENTIAL

Here we briefly review the results obtained in Ref. [5] on the screening of the static potential by a pion gas and ascertain the expected effects of these modifications on quarkonium spectroscopy. Ref. [5] presented a sophisticated calculation of the static quark–anti-quark potential in a pionic medium as a function of the separation of the $Q\overline{Q}$ pair, r, and as a function of the isospin charge, n, of the medium. This required measurement of Wilson loops of various extents in space and in time and to obtain signals for large loops, different levels of HYP (hypercubic) smearing [8] were used in overlapping regions of r, complicating the analysis. As will be discussed below, constructing appropriate ratios of correlation functions was
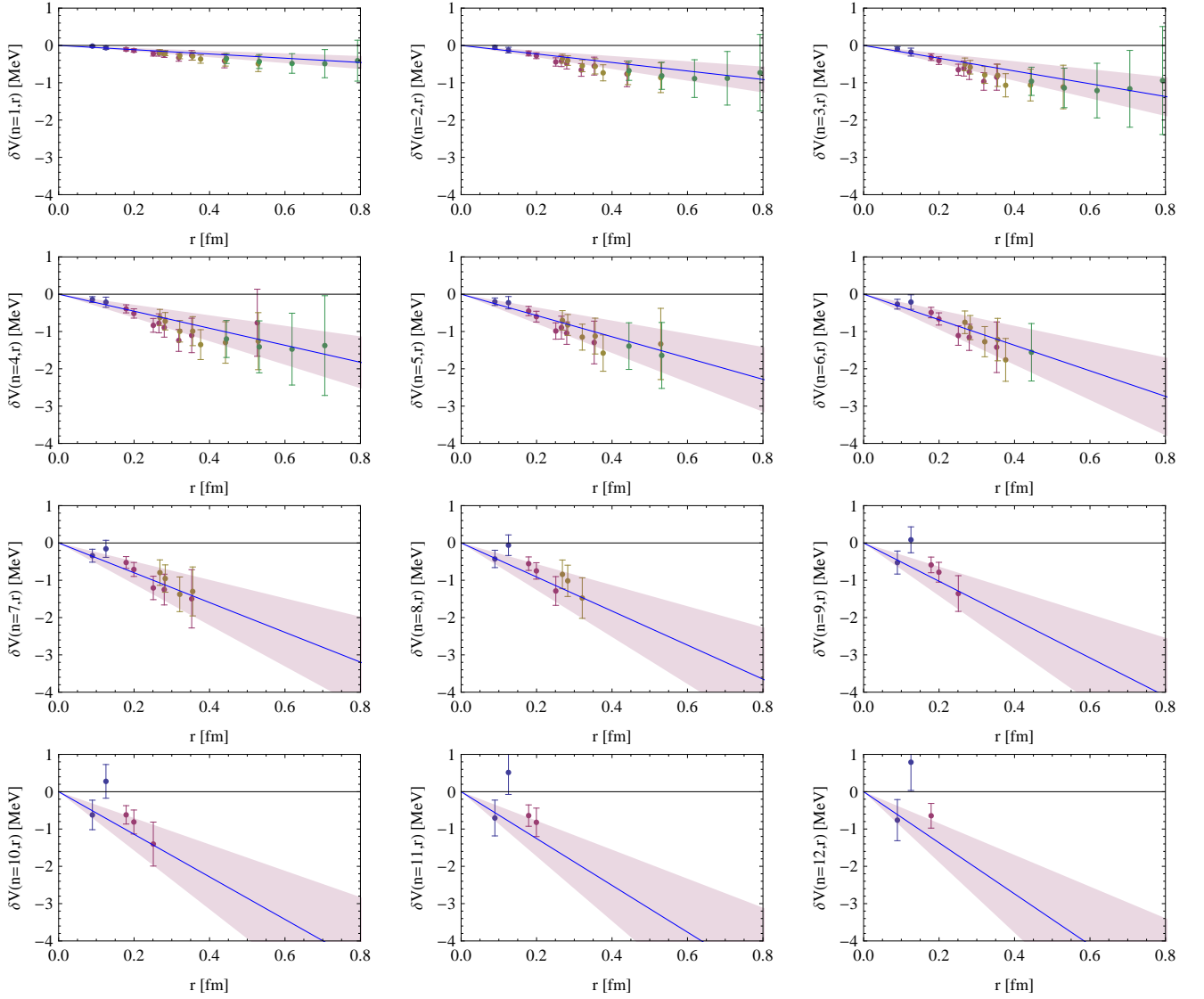
FIG. 1: Shifts in the static potential computed in Ref. [5] fitted to the simple form discussed in the text.

also critical in order to obtain statistically clean measurements. The central results of this work were that the potential is screened by the presence of the medium and that this screening effect is small. For the relatively low pion densities investigated in Ref. [5], the dominant effect corresponded to a change in the potential in the linearly rising region that was approximately linearly dependent on both r and n. This form, $\delta V(\rho_I, r) = \alpha \, \rho_I \, r$, corresponds to the physical expectation of a gas of weakly-interacting pions permeating a flux-tube of constant radius between the static quark and anti-quark, and is a picture in which the appearance of the isospin density, ρ_I, is natural. Performing a correlated fit to the results presented in Ref. [5] using this form, we are able to describe the data well, as shown in Fig. 1, and find that $\alpha = -9.6(1.6)$ MeV fm^2.

To estimate the effects on quarkonium spectroscopy,

we use the Cornell potential $V_{\text{Cornell}}(r) = -(4/3)\alpha_s/r + \kappa \, r$ with $\alpha_s = 0.24$ and $\sqrt{\kappa} = 468$ MeV (values fixed in vacuum from Ref. [9]) and augment it with the small screening shift discussed above. We then solve the radially symmetric Schrödinger equation numerically for angular momentum ℓ and reduced mass $m_{\text{red}} = m/2$ (where m is the heavy-quark mass),

$$\left[-\frac{1}{2m_{\text{red}}} \frac{d^2}{dr^2} + \frac{\ell(\ell+1)}{2m_{\text{red}} \, r^2} \right.$$
$$\left. + V_{\text{Cornell}}(r) + \delta V(\rho_I, r) \right] u_\ell(r) = E \, u_\ell(r), \quad (1)$$

to establish the wave functions and eigenstate energies for the various quantum numbers. The energy shift is then defined simply as the difference of the resulting energy from that where $\delta V(\rho_I, r)$ is omitted. We calculate this shift for both the $1S$ and $1P$ states and various dif-
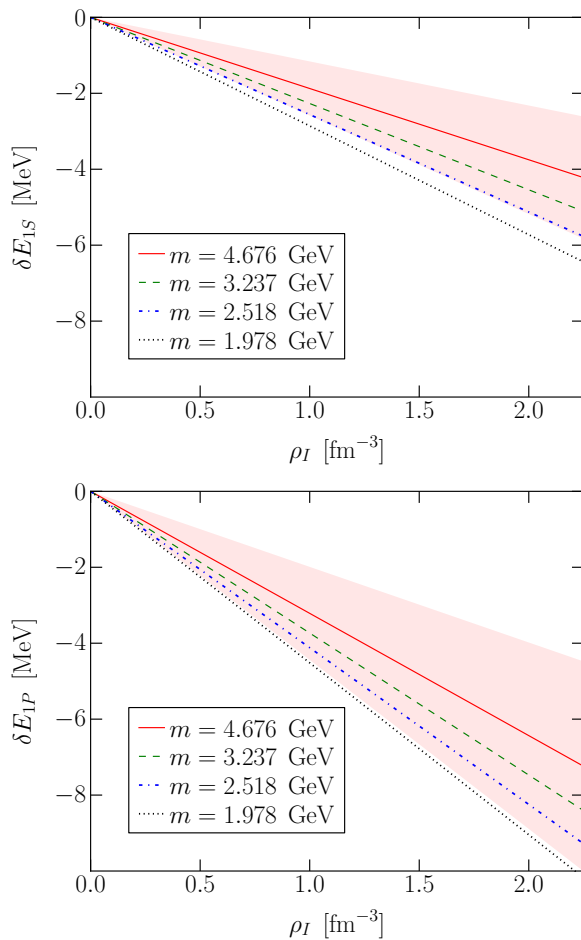
FIG. 2: Shifts in the energies of the $1S$ (upper) and $1P$ (lower) states in quarkonium as a function of the isospin density. Results are shown for four different values of the heavy-quark mass with the uncertainty shown only for the mass closest to the physical bottom-quark mass, $m = 4.676$ GeV (uncertainties for the other masses are of similar size).

ferent values of the heavy-quark mass as shown in Fig. 2. We note that one could use only the Cornell potential to determine the wave functions and include the additional small shift from the screening as a perturbation, calculating

$$\delta E(\rho_I) \sim \int dr \; u_\ell^{(0)*}(r) \delta V(\rho_I, r) u_\ell^{(0)}(r) , \qquad (2)$$

where $u_\ell^{(0)}(r)$ are the solutions to Eq. (1) when $\delta V(\rho_I, r)$ is omitted. As the shift is small, we expect this will give consistent results.

Since P-wave states are more extended in size, they probe regions of the potential where the shift is larger and consequently we find that the energy shift is larger for these states than for the S-wave states. The effect also increases as the heavy-quark mass decreases, again because of the larger size of the lighter systems.

In the following, we determine quarkonium eigenenergies in (NR)QCD at non-zero isospin density and investigate to what extent they are predicted by the potential model described above based on a screening pion gas.

III. LATTICE METHODOLOGY

A. Lattice details

In this study, we make use of anisotropic gauge configurations generated by the Hadron Spectrum and NPLQCD collaborations. The full details of the action and algorithms used to generate the configurations are discussed in the original works, Refs. [10, 11]; here we summarise the salient features of the configurations and the measurements that we perform. A tree-level, tadpole-improved gauge action [12], and $n_f = 2+1$ flavour clover fermion action [13] are used. Two levels of stout smearing [14] with weight $\rho = 0.14$ are applied in spatial directions only in order to preserve the ultra-locality of the action in the temporal direction. The gauge action is constructed without a 1×2 rectangle in the time direction for the same reason. In this study, we make use of a single spatial lattice spacing, $a_s = 0.1227(8)$ fm [11] and have a renormalised anisotropy of $\xi = a_s/a_t = 3.5$, where a_t is the temporal lattice spacing. We also work at a single value of the light-quark mass for this exploratory investigation and use a strange-quark mass that is close to its physical value; these values correspond to a pion mass of $m_\pi \sim 390$ MeV and a kaon mass of $m_K \sim 540$ MeV. For these parameters, we investigate three different ensembles, corresponding to different physical volumes and temporal extents as shown in Table I. The different physical volumes allow us to access a large range of isospin densities in our study, and the different temporal extents provide control of thermal effects as discussed in Ref. [6]. On these gauge configurations we calculate correlation functions involving light quarks and use the colourwave propagator basis introduced in Ref. [6], fixing to Coulomb gauge and using plane-wave sources and sinks for a range of low momenta (N_{mom} in total on each ensemble, see Table I). For each case, we calculate light-quark propagators on N_{cfg} configurations from N_{src} time-slices, equally spaced throughout the temporal extent. Details of the NRQCD heavy quark propagator calculations are discussed below.

$L^3 \times T$	L[fm]	$m_\pi L$	$m_\pi T$	u_{0s}	N_{cfg}	N_{src}	N_{mom}
$16^3 \times 128$	2.0	3.86	8.82	0.7618	334	8	33
$20^3 \times 256$	2.5	4.82	17.64	0.7617	170	16	7
$24^3 \times 128$	3.0	5.79	8.82	0.7617	170	8	19

TABLE I: Details of the ensembles and measurements used in this work. u_{0s} is defined as the fourth root of the spatial plaquette.

B. Multi-pion lattice correlators

In order to produce the medium that will modify the propagation of the quarkonium states, we use the canonical approach of constructing many-pion correlation functions that is described in detail in Ref. [6], using methods developed there and in earlier works [15–19]. As discussed therein, correlators of a fixed isospin charge, $n = \sum_{i=1}^{N} n_i$, and total momentum, $\mathbf{P}_f$, making use of N sources, are given by

$$
\begin{aligned}
C_{n_1,\cdots,n_N}(t, \mathbf{P}_f) &= \langle \mathcal{O}_{n\pi^+}(t) \mathcal{O}^{\dagger}_{n\pi^+}(0) \rangle \\
&= \left\langle \prod_{i=1}^{N} \left(\sum_{\mathbf{x}_i, \mathbf{x}'_i} e^{-i(\mathbf{p}_1^i \mathbf{x}_i - \mathbf{p}_2^i \mathbf{x}'_i)} \overline{d}(\mathbf{x}'_i, t)\gamma_5 u(\mathbf{x}_i, t) \right)^{n_i} \right. \\
&\quad \left. \times \prod_{j=1}^{n} \left(\sum_{\mathbf{y}_j} e^{i\mathbf{p}_{f_j}\mathbf{y}_j} \overline{u}(\mathbf{y}_j, 0)\gamma_5 d(\mathbf{y}_j, 0) \right) \right\rangle, \quad (3)
\end{aligned}
$$

where $\mathbf{P}_f = \sum_{i=1}^{n} \mathbf{p}_{f_i}$, and, for momentum conservation, $\sum_{i=1}^{N}(\mathbf{p}_1^i - \mathbf{p}_2^i) = \sum_{j=1}^{n} \mathbf{p}_{f_j}$. In what follows, we will set $\mathbf{P}_f = 0$ but the $\mathbf{p}_{f_i}$ and $\mathbf{p}_{1,2}^i$ take various values subject to these constraints; different choices of the momenta defining the interpolating operators will have different overlap onto the eigenstates of the chosen $\mathbf{P}_f$ but provide additional statistical resolution in the determination of the energy of the system.

To construct these correlation functions, we work in Coulomb gauge and compute light-quark colourwave propagators

$$
S_{u/d}(\mathbf{p}, t; \mathbf{p}', 0) = \sum_{\mathbf{x}} e^{-i\mathbf{p}\mathbf{x}} S_{u/d}(\mathbf{x}, t; \mathbf{p}', 0), \quad (4)
$$

where

$$
S_{u/d}(\mathbf{x}, t; \mathbf{p}', 0) = \sum_{\mathbf{y}} e^{i\mathbf{p}'\mathbf{y}} S_{u/d}(\mathbf{x}, t; \mathbf{y}, 0)
$$

is a solution of the lattice Dirac equation:

$$
\sum_{\mathbf{x}, t} D(\mathbf{y}, \tilde{t}; \mathbf{x}, t) S_{u/d}(\mathbf{x}, t; \mathbf{p}', 0) = e^{i\mathbf{p}'\mathbf{y}} \delta_{\tilde{t}, 0}.
$$

The contractions implicit in Eq. (3) can be written in terms of a matrix $\tilde{A}$, the 12×12 sub-blocks of which are given by

$$
\tilde{A}_{k,i}(t) = \sum_{\mathbf{p}} S\left(\mathbf{p}_1^k, \mathbf{p}\right) S^{\dagger}\left(-\mathbf{p}_2^i, \mathbf{p}_{f_i} - \mathbf{p}\right), \quad (5)
$$

where k, i label the source and sink, and the dependence on $\mathbf{p}_1^k$, $\mathbf{p}_2^i$, and $\mathbf{P}_f$ is suppressed. The correlators above can be extracted by noting that combinations of the $C_{n_1,\cdots,n_N}$ for a given $n = \sum_{i=1}^{N} n_i$ are the coefficients of the expansion of

$$
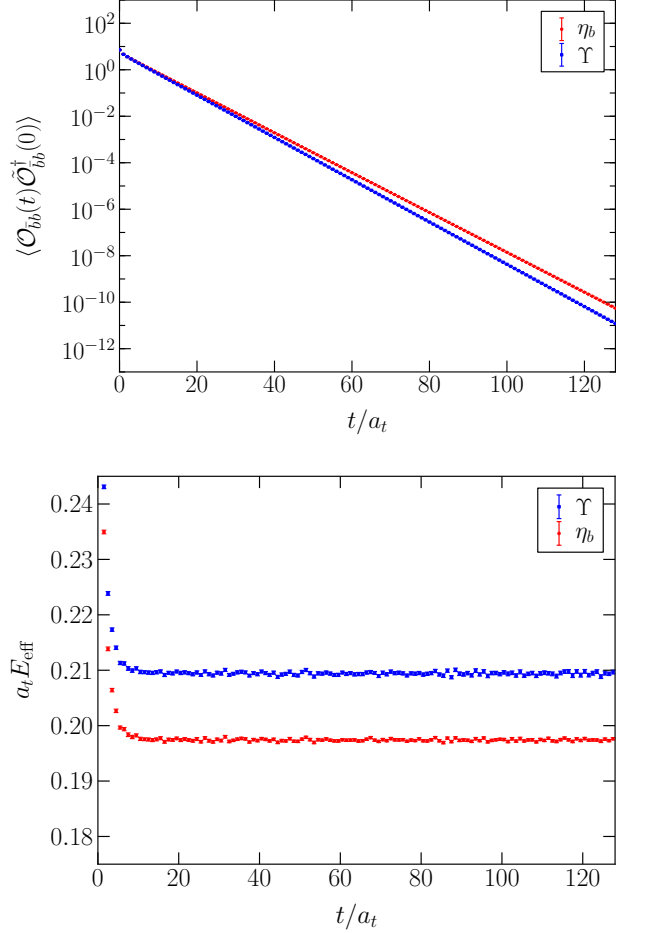\det[1 + \lambda\tilde{A}] = 1 + \lambda C_{1\pi} + \lambda^2 C_{2\pi} + \cdots + \lambda^{12N} C_{12N\pi}, \quad (6)
$$

FIG. 3: η_b and Υ correlators (upper) and effective energies (lower) on the $20^3 \times 256$ ensemble, for $a_s m = 2.6$.

and can be computed efficiently using the methods of Ref. [6]. The different $C_{n_1,\cdots,n_N}$ for a given n occur in complicated combinations in this expansion, however we are explicitly only interested in the energies of the system, so the particulars of the combination are irrelevant.

These correlators have been studied in detail in previous work [6] and we do not present them again here. As investigated in detail in Ref. [6], many-pion correlations contain thermal contributions in which parts of the system propagate around the temporal boundary. In our choice of fitting ranges in the analysis presented below, we are careful to remain away from the regions in Euclidean time that are contaminated by either excited states or by these thermal effects.

C. NRQCD for quarkonium correlators

To implement the heavy quarks in our quarkonia systems, we use a lattice discretisation of non-relativistic QCD (NRQCD). Since our light quark and gluon degrees of freedom are defined on an anisotropic lattice,
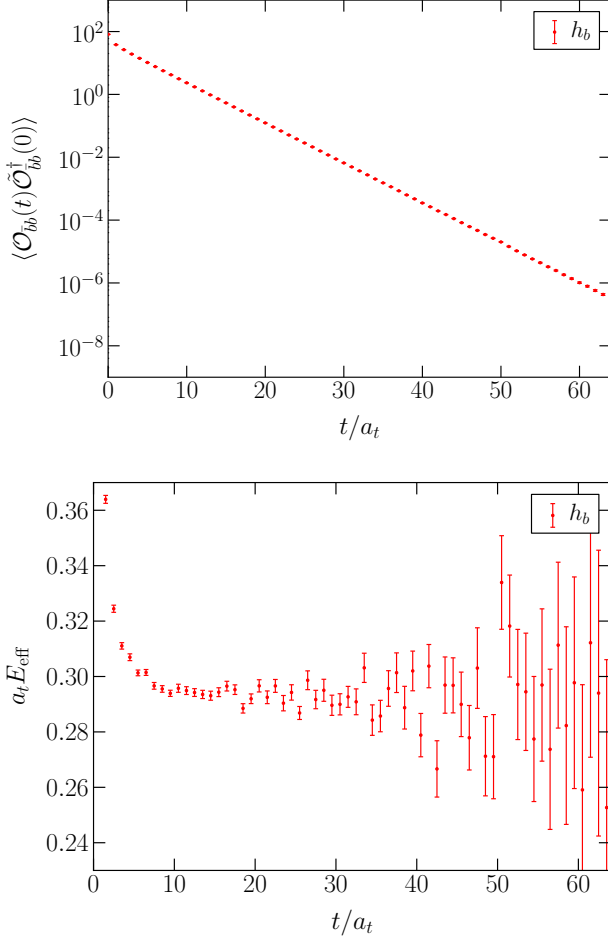
FIG. 4: h_b correlator (upper) and effective energy (lower) on the $16^3 \times 128$ ensemble, for $a_s m = 2.6$.

we require lattice NRQCD [20, 21] formulated on an anisotropic lattice as first set out in Ref. [22]. As the non-relativistic nature of the theory already separates space and time, using a temporal lattice spacing that differs from the spatial lattice spacing is a very natural choice for NRQCD. Anisotropic lattice NRQCD has been used for example to calculate the spectrum of quarkonium hybrid states [23, 24], and recently also to study quarkonium at non-zero temperature [4, 25].

The Euclidean action for the heavy quark field, ψ, can be written as

$$S_\psi = a_s^3 \sum_{\mathbf{x},t} \psi^\dagger(\mathbf{x},t) \left[\psi(\mathbf{x},t) - K(t)\, \psi(\mathbf{x}, t - a_t) \right], \quad (7)$$

where $K(t)$ is the operator that evolves the heavy-quark Green function forward one step in time. Here we use the form

$$K(t) = \left(1 - \frac{a_t\, \delta H|_t}{2} \right) \left(1 - \frac{a_t H_0|_t}{2n} \right)^n U_0^\dagger(t - a_t)$$

$$\times \left(1 - \frac{a_t H_0|_{t-a_t}}{2n} \right)^n \left(1 - \frac{a_t\, \delta H|_{t-a_t}}{2} \right), \quad (8)$$

where U_0 are the temporal gauge links. In this expression,

$$H_0 = -\frac{\Delta^{(2)}}{2m}, \quad (9)$$

is the order-v^2 term in the NRQCD velocity expansion, and δH is a correction term given by

$$\begin{aligned}
\delta H &= -c_1 \frac{\left(\Delta^{(2)}\right)^2}{8m^3} + c_2 \frac{ig}{8m^2} \left(\boldsymbol{\nabla} \cdot \widetilde{\mathbf{E}} - \widetilde{\mathbf{E}} \cdot \boldsymbol{\nabla} \right) \\
&\quad - c_3 \frac{g}{8m^2} \boldsymbol{\sigma} \cdot \left(\widetilde{\boldsymbol{\nabla}} \times \widetilde{\mathbf{E}} - \widetilde{\mathbf{E}} \times \widetilde{\boldsymbol{\nabla}} \right) - c_4 \frac{g}{2m} \boldsymbol{\sigma} \cdot \widetilde{\mathbf{B}} \\
&\quad + c_5 \frac{a_s^2 \Delta^{(4)}}{24m} - c_6 \frac{a_t \left(\Delta^{(2)}\right)^2}{16n\, m^2}
\end{aligned} \quad (10)$$

(the notation is as in Ref. [26]). The operators with coefficients c_1 through c_4 are the relativistic corrections of order v^4, the operator with coefficient c_5 removes the order-a_s^2 discretization error of H_0, and the operator with c_6 removes the leading order-a_t error in the time evolution. We use the tree-level values of the matching coefficients, $c_i = 1$. For tadpole improvement [27] of the derivatives and field strengths, we set u_{0s} equal to the 4th root of the spatial plaquette (see Table I), and set $u_{0t} = 1$.

To avoid instabilities in the time evolution with the operator in Eq. (8), the parameter n must be chosen such that $\max[a_t H_0/(2n)] < 2$ [21]. On an anisotropic lattice, this requires

$$n > 3a_t/(2a_s^2 m) = 3/(2\xi a_s m) \quad (11)$$

(interactions with gluons weaken this requirement slightly [21]). In this work, we set the bare heavy-quark mass to $a_s m = 2.6$ (which is near the b quark mass) as well as to the lower values $a_s m = 1.8, 1.4, 1.1$. Because we have $\xi = 3.5$, a stability parameter of $n = 1$ is sufficient in all cases.

When using NRQCD, all quarkonium energies are shifted by an unknown constant (which is approximately equal to two times the heavy-quark mass). This shift is state-independent and cancels in energy splittings as well as in differences between energies extracted at zero and non-zero isospin density. For the purpose of tuning the heavy-quark mass, we measure the kinetic masses of the η_b and Υ states, defined as

$$a_t M_{\mathrm{kin}} = \frac{(a_s \mathbf{p})^2/\xi^2 - [a_t E(\mathbf{p}) - a_t E(0)]^2}{2\left[a_t E(\mathbf{p}) - a_t E(0)\right]}, \quad (12)$$

with one unit of lattice momentum, $|\mathbf{p}| = 2\pi/L$. The spin-averaged values of the $1S$ kinetic masses, $\overline{M_{\mathrm{kin}}} = (3M_{\mathrm{kin}}^\Upsilon + M_{\mathrm{kin}}^{\eta_b})/4$ computed on the $16^3 \times 128$ ensemble (at $\rho_I = 0$), are given in Table II.

In the main calculations of this work, we use zero-momentum smeared quarkonium interpolating fields of the form

$$\mathcal{O}_{\bar{b}b}(t) = \sum_{\mathbf{y}'} \sum_{\mathbf{y}} \chi^\dagger(\mathbf{y}', t) \Gamma(\mathbf{y} - \mathbf{y}') \psi(\mathbf{y}, t) \quad (13)$$

$a_s m$	$a_t \overline{M}_{\rm kin}$	$\overline{M}_{\rm kin}$ (GeV)
1.1	0.8732(49)	4.915(42)
1.4	1.0138(20)	5.706(39)
1.8	1.2225(15)	6.881(46)
2.6	1.6590(12)	9.337(62)

TABLE II: Spin-averaged quarkonium kinetic masses on the $16^3 \times 128$ ensemble.

at the sink and

$$\tilde{\mathcal{O}}_{\bar{b}b}(0) = \sum_{\mathbf{x}} \chi^{\dagger}(\mathbf{0},0)\Gamma(\mathbf{x})\psi(\mathbf{x},0) \qquad (14)$$

at the source. Here, χ is the heavy anti-quark field and $\Gamma(\mathbf{r})$ is the smearing function, which is a 2×2 matrix in spinor space. Note that antiquark propagators can be obtained from quark propagators through $G_{\chi}(x,x') = -G_{\psi}(x',x)^{\dagger}$. The quantum numbers of the quarkonium interpolating fields considered in this work are listed in Table III. To optimize the overlap with the $1S$ and $1P$ ground states we use wave functions from a lattice potential model (see Appendix D of Ref. [26]) in the construction of $\Gamma(\mathbf{r})$ (as already mentioned in the previous section, the gauge configurations are fixed to Coulomb gauge). The heavy-quark mass used in the potential model is adjusted to match the mass used in the lattice QCD calculation. We use $\Gamma(\mathbf{x})$ as the source for the quark propagator and a point source for the antiquark. At the sink, the convolution in Eq. (13) is performed efficiently using fast Fourier transforms.

In order to reach the high statistical accuracy needed to extract the small effects of the isospin charge density, we compute quarkonium two-point functions for 64 different spatial source locations (distributed on a cubic sub-lattice with spacing $L/4$ on each of the source time slices, and average over these source locations. Examples of free quarkonium two-point functions with the smearing technique discussed above are given in Figs. 3 and 4. Note that ground-state plateaus are reached already at a distance of ~ 0.4 fm in Euclidean time, which demonstrates the efficiency of the smearing technique used here.

Name	$\mathcal{R}^{PC}$	$\Gamma(\mathbf{r})$
η_b	A_1^{-+}	$\phi_{1S}(\mathbf{r})$
Υ	T_1^{--}	$\phi_{1S}(\mathbf{r})\,\sigma_j$
h_b	T_1^{+-}	$\phi_{1P}(\mathbf{r},j)$
χ_{b0}	A_1^{++}	$\sum_j \phi_{1P}(\mathbf{r},j)\,\sigma_j$
χ_{b1}	T_1^{++}	$\sum_{k,l}\epsilon_{jkl}\,\phi_{1P}(\mathbf{r},k)\,\sigma_l$
χ_{b2}	T_2^{++}	$\phi_{1P}(\mathbf{r},j)\,\sigma_k + \phi_{1P}(\mathbf{r},k)\,\sigma_j$ (with $j \neq k$)

TABLE III: Smearing functions $\Gamma(\mathbf{r})$ used in the quarkonium interpolating fields for the given representation of the cubic group, $\mathcal{R}$ and values of parity, P, and charge-conjugation, C. The functions $\phi_{1S}(\mathbf{r})$ and $\phi_{1P}(\mathbf{r},j)$ are eigenfunctions from a lattice potential model.
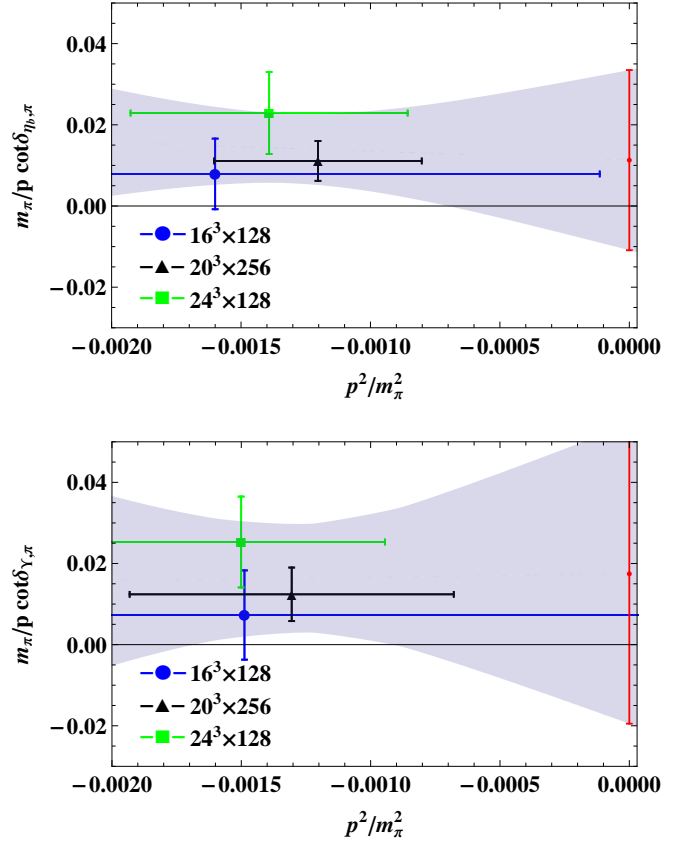

FIG. 5: Extracted inverse phase shifts for η_b–π and Υ–π scattering. Fitting the phase shift to $p \cot\delta(p)/m_\pi = -\frac{1}{m_\pi a} + \frac{m_\pi r}{2}\frac{p^2}{m_\pi^2}$, as shown by the shaded band, we can extract the scattering length shown by the point at $p^2/m_\pi^2 = 0$.

D. Correlator ratios for energy shifts

To investigate the effect of the medium on quarkonium propagation, we consider the correlators

$$C(n;\bar{b}b;t) = \langle \mathcal{O}_{\bar{b}b}(t)\mathcal{O}_{n\pi^+}(t)\tilde{\mathcal{O}}_{\bar{b}b}^{\dagger}(0)\mathcal{O}_{n\pi^+}^{\dagger}(0)\rangle, \quad (15)$$

where $\langle\ldots\rangle$ denotes path integration via the average over our ensembles of gauge configurations, and the interpolators $\mathcal{O}_{n\pi^+}^{\dagger}$ and $\mathcal{O}_{\bar{b}b}^{\dagger}$ produce the quantum numbers of n-pion and $\bar{b}b$ states as discussed in the preceding sub-sections. States with the combined quantum numbers of the given quarkonium state ($\bar{b}b = \eta_b$, Υ, h_b, χ_{b0}, χ_{b1}, χ_{b2}) and the n-pion system propagate in this correlator and naturally, the spectrum of this system is different from the sum of the spectra of n pions and of quarkonium because of interactions. At Euclidean times where only the ground state of the system is resolved (after excited states have decayed and before thermal states are manifest), this correlator will decay exponentially as

$$C(n;\bar{b}b;t) \longrightarrow \tilde{Z}_{n;\bar{b}b}\exp(-E_{n;\bar{b}b}t), \qquad (16)$$

where $E_{n;\bar{b}b}$ is the ground-state energy of the combined system.

To access the change in the quarkonium energy as a function of isospin density or chemical potential, we further construct the ratios

$$R(n, \bar{b}b; t) = \frac{\langle \mathcal{O}_{\bar{b}b}(t)\mathcal{O}_{n\pi^+}(t)\tilde{\mathcal{O}}_{\bar{b}b}^\dagger(0)\mathcal{O}_{n\pi^+}^\dagger(0)\rangle}{\langle \mathcal{O}_{\bar{b}b}(t)\tilde{\mathcal{O}}_{\bar{b}b}^\dagger(0)\rangle\langle \mathcal{O}_{n\pi^+}(t)\mathcal{O}_{n\pi^+}^\dagger(0)\rangle} . \quad (17)$$

Since the two terms in the denominator decay exponentially at large times as $\exp(-E_{\bar{b}b}t)$ and $\exp(-E_{n\pi^+}t)$ respectively, the ratio will behave as

$$R(n; \bar{b}b; t) \longrightarrow Z_{n;\bar{b}b} \exp(-\Delta E_{n;\bar{b}b}t) + \dots , \quad (18)$$

where $\Delta E_{n;\bar{b}b} = E_{n;\bar{b}b} - E_{n\pi^+} - E_{\bar{b}b}$ is the quantity of central interest in our investigation.

IV.   QUARKONIUM–PION SCATTERING

The quarkonium state in the presence of a single pion allows us to study the scattering phase shift of this two-body system using the finite-volume formalism developed by Lüscher [28, 29]. The S-wave quarkonium states we consider have angular momentum $J = 0, 1$ and define the total angular momentum of the entire system since the pion is spin-zero. Since the pion and $\bar{b}b$ states have different masses, the appropriate generalisation of the Lüscher relation to asymmetric systems [30] is required. We can define a scattering momentum $p = |\mathbf{p}|$ through the relation

$$\sqrt{|a_s\mathbf{p}|^2/\xi^2 + a_t^2 M_{\bar{b}b}^2} + \sqrt{|a_s\mathbf{p}|^2/\xi^2 + a_t^2 M_\pi^2} \quad (19)$$
$$= a_t \Delta E_{\bar{b}b,\pi} + a_t M_{\bar{b}b} + a_t M_\pi ,$$

where $M_{\bar{b}b} \equiv M_{\text{kin}}^{\bar{b}b}$ is the kinetic mass of the $\bar{b}b$ state. The scattering momentum then determines the eigenvalue equation

$$p \cot \delta_{\bar{b}b,\pi}(p) = \frac{1}{\pi L}\mathbf{S}\left(\frac{p^2 L^2}{4\pi^2}\right), \quad (20)$$

$$\mathbf{S}(x) = \lim_{\Lambda\to\infty}\left[\sum_{\mathbf{n}\neq 0}^{|\mathbf{n}|<\Lambda}\frac{1}{|\mathbf{n}|^2 + x} - 4\pi\Lambda\right], (21)$$

that is satisfied by the $\bar{b}b$–π scattering phase shift, $\delta_{\bar{b}b,\pi}(p)$, at the scattering momentum.

Since we have three different lattice volumes, we can extract the phase shift at multiple momenta. In Figure 5, we show the phase shifts that we extract for the η_b–π and Υ–π scattering channels. These interactions necessarily vanish in the chiral limit as the quarkonium states are chiral singlet objects. We therefore expect only small scattering phase shifts at the quark masses considered in our study. At the level of statistical precision we have achieved, we can barely resolve the phase shifts from zero,

but they are indeed found to be small. The measured values of the S-wave phase shifts are given in Tables IV and V, while for the P-wave states we are unable to extract statistically meaningful results. Since the measured scattering momenta are small, it is possible to perform a fit to the effective-range expansion

$$p \cot \delta(p)/m_\pi = -\frac{1}{m_\pi a} + \frac{m_\pi r}{2}\frac{p^2}{m_\pi^2} + \dots , \quad (22)$$

to extract the scattering length and effective range for these interactions. This extrapolation is shown in Fig. 5 and results in $m_\pi a_{\eta_b,\pi} = 0.011(22)$ and $m_\pi r_{\eta_b,\pi} = -4(17)$ for the η_b state, and $m_\pi a_{\Upsilon,\pi} = 0.017(37)$ and $m_\pi r_{\Upsilon,\pi} = 2(29)$ in the case of the Υ. Clearly the interactions are extremely weak but are at the limits of our ability to resolve with current statistics.

TABLE IV: The η_b–π phase shifts extracted using the Lüscher method as described in the main text.

$V^3 \times T$	p^2/m_π^2	$(p\cot\delta(p))^{-1}$[fm]	$m_\pi/(p\cot\delta(p))$
$16^3 \times 128$	$-0.0016(15)$	$0.0040(44)$	$0.0079(87)$
$20^3 \times 256$	$-0.0012(4)$	$0.0056(25)$	$0.0111(49)$
$24^3 \times 128$	$-0.0014(5)$	$0.0116(51)$	$0.0229(101)$

TABLE V: The Υ–π phase shifts extracted using the Lüscher method as described in the main text.

$V^3 \times T$	p^2/m_π^2	$(p\cot\delta(p))^{-1}$[fm]	$m_\pi/(p\cot\delta(p))$
$16^3 \times 128$	$-0.0015(18)$	$0.0037(56)$	$0.0073(110)$
$20^3 \times 256$	$-0.0013(6)$	$0.0063(34)$	$0.0124(66)$
$24^3 \times 128$	$-0.0015(6)$	$0.0128(57)$	$0.0253(112)$

V.   ISOSPIN DENSITY DEPENDENCE OF QUARKONIUM

For larger isospin charge, we interpret the system of pions in terms of a medium of varying isospin charge density once the ground state is reached. In the correlators $C(n; \bar{b}b; t)$, the quarkonium state exists in this medium, interacting with it. We consider first the S-wave quarkonium states as they are statistically better resolved than P-wave states.

A.   S-wave states

The correlators $C(n, \bar{b}b, t)$ are shown in Fig. 6 for $\bar{b}b = \Upsilon$ at representative values of the isospin charge

and for $a_s m = 2.6$ on the $20^3 \times 256$ and $16^3 \times 128$ ensembles. The in-medium correlators on the $20^3 \times 256$ ensemble exhibit a long region of Euclidean time in which they decay as a single exponential. This region overlaps with the regions in which the multi-pion correlators and the individual quarkonium correlators are saturated by their respective ground states. This gives us confidence that by considering the correlator ratios of Eq. (17) we can legitimately extract the quarkonium energy shifts in medium. On the ensembles with $T = 128$, thermal contamination is more significant and restricts the range of useful time-slices, particularly for large isospin charge.

The correlator ratios, $R(n, \bar{b}b; t)$, discussed above, are shown for both Υ and η_b at a heavy quark mass $a_s m = 2.6$ on the $20^3 \times 256$ ensemble for a range of different isospin charges, $n = 6$, 12, and 18, in Figs. 7 and 8 along with fits to time dependence using Eq. (18). Fits are performed over a range of times where both the individual multi-pion correlation functions and quarkonium correlation functions exhibit ground-state saturation and are free from thermal (backward propagating) state contamination. This is ensured by choosing the central fit range $[t_{\min}, t_{\max}]$ such that a fit over the range $[t_{\min}-5, t_{\max}+5]$ has an acceptable quality of fit. On the $20^3 \times 256$ ensemble, we choose $t_{\min} = 20$ and $t_{\max} = 80$, beyond which thermal contributions are apparent. Because thermal contributions are more significant for the ensembles with $T = 128$, we choose $t_{\max} = 40$ for these cases. Statistical uncertainties are estimated using the bootstrap procedure. To estimate the systematic uncertainties of the fits, we calculate the standard deviation between the three energies extracted from fits with the ranges $[t_{\min} - 5, t_{\max} - 5]$, $[t_{\min}, t_{\max}]$, and $[t_{\min} + 5, t_{\max} + 5]$ on each bootstrap sample. The systematic uncertainty is then obtained as the average of this standard deviation over the bootstrap samples.

The extracted energy shifts and uncertainties are shown in Table VI. For larger values of n, the energy shifts become noisier and we limit our analysis to the range of isospin densities where a successful fit could be performed for a given ensemble.

As a check of the methods of our study, we construct ratios in which we artificially remove the correlations between the $\bar{b}b$ system and the many-pion state by evaluating $\sum_c C_{\bar{b}b}(c) C_{n\pi}(c + \delta c)$, where $C_X(c)$ represents the correlation function for the quantity X measured on configuration c, and δc is either a constant displacement or a random shift. In both cases, the removal of the correlation eliminates the signal for an energy shift. This is shown for the η_b with $n = 5$ in Fig. 9 for random shifts, and the same qualitative effect is seen for all choices of the density and quarkonium state that are considered.

To summarise the analysis of the correlator ratios for the S-wave quarkonium states, Fig. 10 shows the isospin density dependence of the energy shift of the $\bar{b}b$ states from the free $\bar{b}b$ energy for both the Υ and η_b channels. Results are presented for the ranges of isospin charge density where a statistically meaningful extraction of the

energy shift can be made. As can be seen, there is a significant negative energy shift for much of the range of isospin density that we have investigated. The magnitude of this shift first increases as the isospin density is increased, before saturating at a value of about 1 MeV and finally decreasing to zero for large ρ_I, albeit with increasing uncertainty. It is interesting to note that the saturation occurs at the point at which a marked change in the energy density of the many-pion system was observed in Ref. [6], and is likely caused by the changing nature of the screening medium at this point. The behaviour at low densities is in line with the expectations of the potential model discussed earlier, but the saturation effect is not predicted (the model was developed using the measured shifts in the potential in the low density region, so this is not surprising).

We have performed these calculations for all three ensembles of configurations but have only been able to access a limited range of densities with the current statistical precision. The results from all of the ensembles are consistent in the region in which they overlap. The $16^3 \times 128$ ensemble provides the largest density range.

We also consider the shifts in the splitting between the η_b and Υ energies in medium as a function of the density. We extract these shifts by calculating the correlated differences between the individual energies using the bootstrap method. A summary of the isospin charge dependence of this splitting is shown in Fig.11. There are hints that the Υ energy is shifted slightly more than the η_b energy by the presence of the medium. However, the smallest-volume data do not show this difference and it may not be significant.

B. P-wave states

We also analyse the lowest-energy P-wave quarkonium states, h_b, χ_{b0}, χ_{b1} and χ_{b2}, in medium. We find that we cannot resolve differences between the medium effects for these different states and so consider a spin average of their energies. It order to extract this average energy, we construct the product correlator

$$C_P = C_{h_b}^{\frac{3}{12}} C_{\chi_{b0}}^{\frac{1}{12}} C_{\chi_{b1}}^{\frac{3}{12}} C_{\chi_{b2}}^{\frac{5}{12}} , \qquad (23)$$

that decays with the average energy $E_{n,P} = \frac{1}{12}[3E_{n,h_b} + E_{n,\chi_{b0}} + 3E_{n,\chi_{b1}} + 5E_{n,\chi_{b2}}]$ (in the above expression $C_{\bar{b}b}^J$ is short-hand notation for $[C(n, \bar{b}b; t)]^J$). We also consider the analogous S-wave spin average combination

$$C_S = C_{\eta_b}^{\frac{1}{4}} C_{\Upsilon}^{\frac{3}{4}} . \qquad (24)$$

These can be used to form correlator ratios, $R(n, P; t)$ and $R(n, S; t)$, analogous to Eq. (17). Since the P-wave quarkonium correlators are themselves statistically noisier than the S-wave correlators (see Figs. 3 and 4), the precision with which we can extract the P-wave energy shifts is reduced. In our fits to these correlators, we
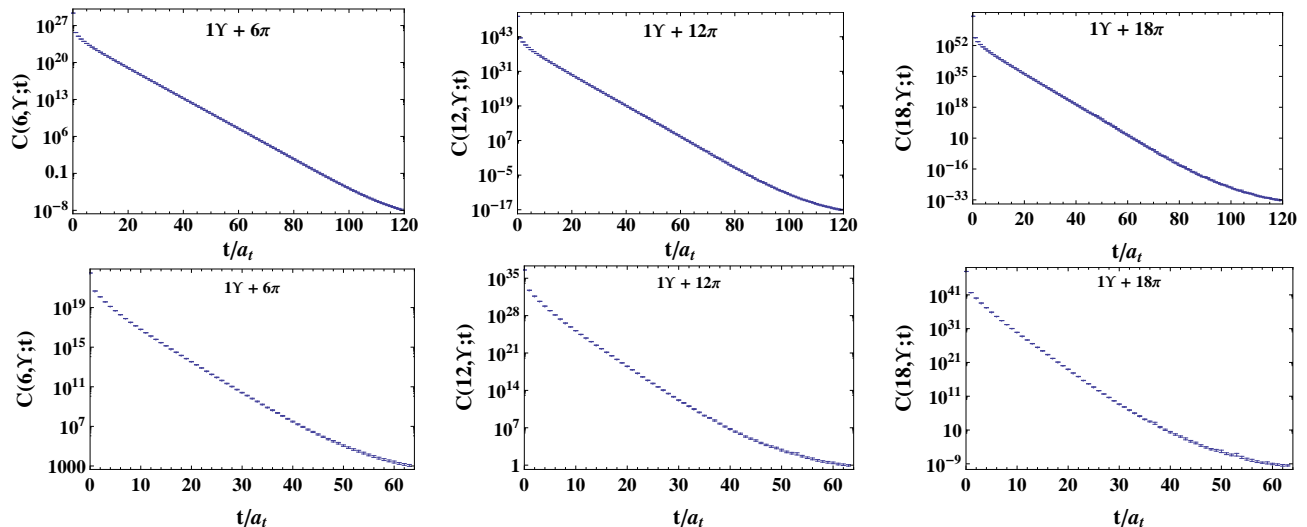
FIG. 6: The correlators for the Υ in a medium corresponding to isospin charge n for $n = 6$, 12, and 18 are shown. Data are presented for $a_s m = 2.6$ on the $20^3 \times 256$ (upper) and $16^3 \times 128$ (lower) ensembles. Correlators for the η_b in medium behave similarly.

choose $t_{\min} = 15$ and $t_{\max} = 35$. Fig. 12 shows representative correlators and correlator ratios for the spin average P−wave state, and Fig. 13 summarises the measured shift, also showing the spin averaged S-wave shift for comparison. The potential model expectation is that the P-wave shift will be larger than the S-wave shift; to investigate this, we form correlated differences between the individual S- and P-wave shifts but the statistical uncertainty remains large and we are unable to resolve a difference.

C. Heavy-quark mass dependence

As discussed in Section III C, we have performed calculations for four different values of the heavy-quark mass, $a_s m$, ranging from the bottom-quark mass down to ~ 1.5 times the charm-quark mass. The analysis of the in-medium correlators and ratios is very similar for all masses and we do not present it in detail. To investigate the variation of the energy shifts as a function of the heavy-quark mass we compute $\Delta E_{n,\bar{b}b}(a_s m) - \Delta E_{n,\bar{b}b}(a_s m = 2.6)$ using the bootstrap method. Because of correlations between the measurements for different values of the heavy-quark mass, this provides a more statistically precise determination of the difference than would be evident from a naive comparison. Figure 14 shows these energy differences for the different values of $a_s m$. It is apparent that the strength of the energy shift in both η_b and Υ increases as the heavy-quark mass decreases, in line with expectations from the potential model discussed above. Since the quarkonium states for lower heavy-quark masses are physically larger, they probe regions of larger quark–anti-quark separation

where the potential shift is more significant.

VI. DISCUSSION

Heavy-quark bound states provide an important probe of the properties of a medium and have been used in this work to investigate systems of large isospin charge density created by many-pion correlators. Specifically, we have used lattice QCD to investigate how the presence of this medium modifies the NRQCD energies of various quarkonium states. Our calculations make use of ensembles of lattices with three different physical volumes at a single lattice spacing and at a single light quark mass corresponding to $m_\pi \sim 390$ MeV. We have found a measurable decrease in the energy of both the η_b and Υ states and in the spin-averaged P-wave energy. This decrease grows as the isospin charge increases before plateauing at a charge density at which Ref. [6] previously observed strongly non-monotonic behaviour of the energy density of the medium. The saturation of the energy shift provides further support to the conjecture that a transition from a pion gas to a Bose-Einstein condensate of pions occurs at this point. In the region of low isospin density where the energy shift is increasing, the quarkonium energy shifts are found to be qualitatively in agreement with our expectations from a potential model augmented with the hadronic screening effect found in Ref. [18].

We have investigated how the observed energy shifts depend on the mass of the heavy quark–anti-quark pair, finding an enhanced effect for lighter masses. Given the phenomenological interest in J/Ψ suppression in medium, it will be interesting to investigate the analogous behaviour in the charmonium sector using alterna-
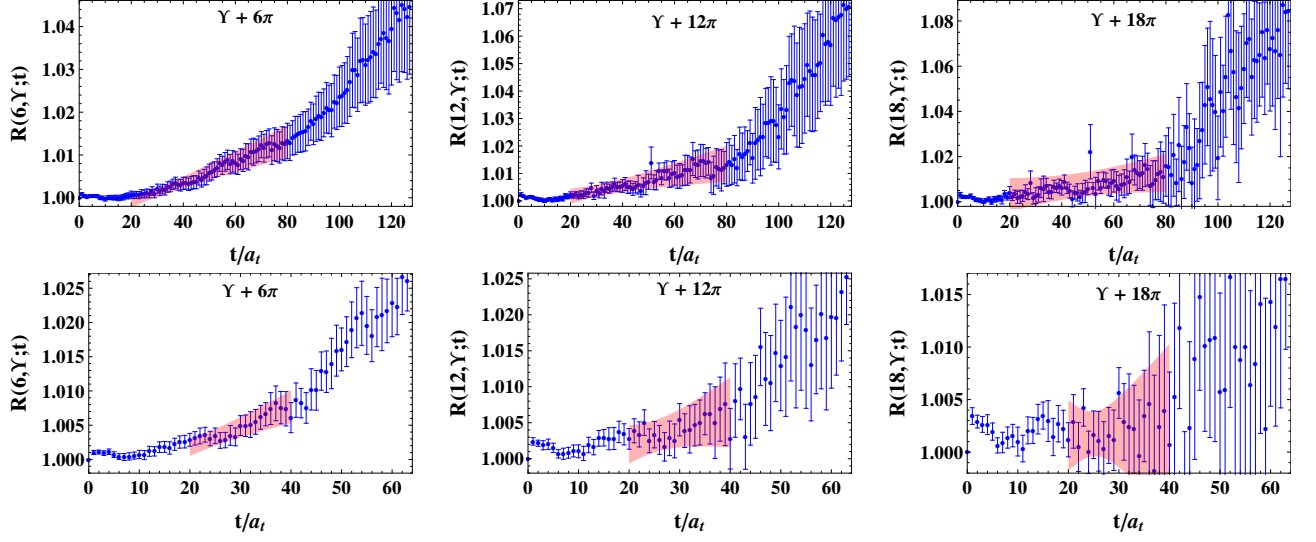
FIG. 7: The correlator ratios for the Υ in a medium corresponding to isospin charges $n = 6, 12, 18$. The shaded bands show the statistical uncertainties of fits of the form given in Eq. (18). Data are shown for $a_s m = 2.6$ on the $20^3 \times 256$ (upper) and $16^3 \times 128$ (lower) ensembles.
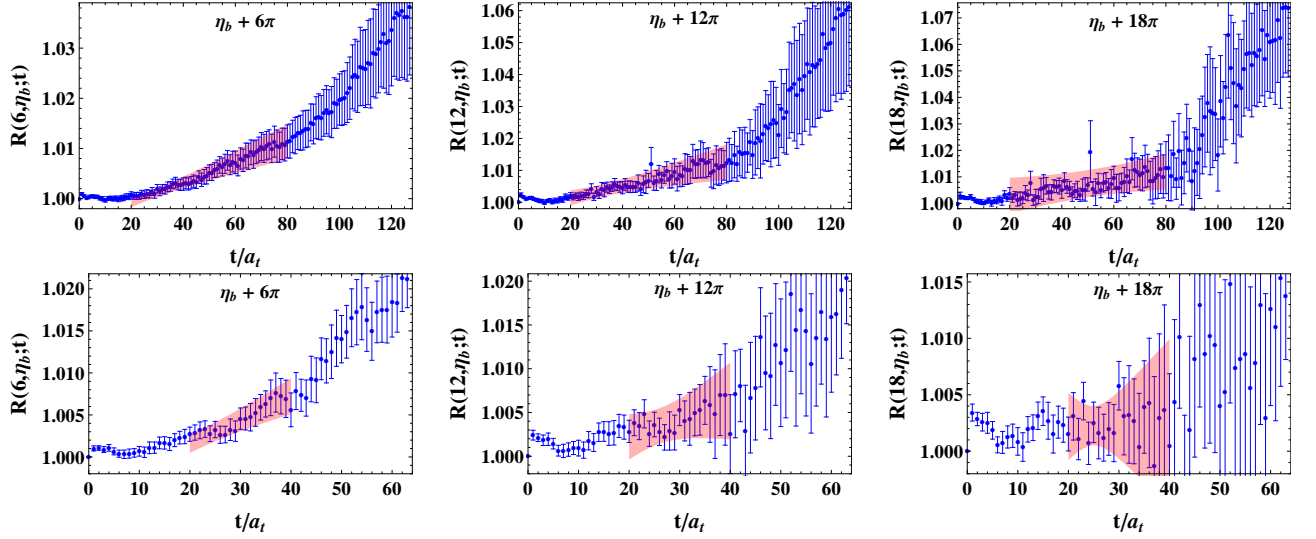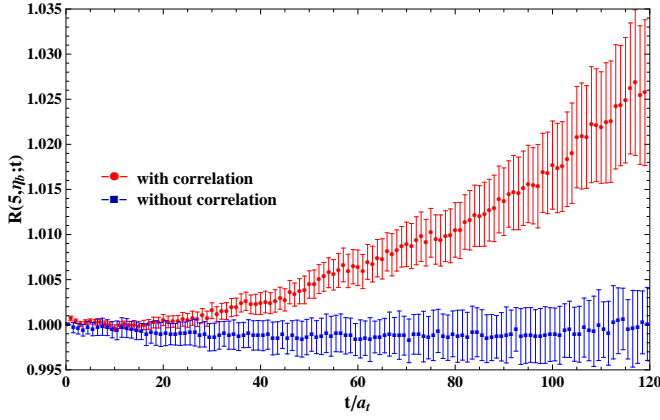

FIG. 8: The correlator ratios for the η_b in a medium corresponding to isospin charges $n = 6, 12, 18$. The shaded bands show the statistical uncertainties of fits of the form given in Eq. (18). Data are shown for $a_s m = 2.6$ on the $20^3 \times 256$ (upper) and $16^3 \times 128$ (lower) ensembles.

FIG. 9: The ratio $R(5, \eta_b; t)$ computed with and without the correct correlation between the η_b and many-pion system on the $20^3 \times 256$ ensemble, as discussed in the main text. The shift (difference from unity) is only apparent when correlations are included.

tive formulations of the heavy-quark action more appropriate for the charm quark. However, this is beyond the scope of the current work.

A similar study of NRQCD quarkonium correlators in QC$_2$D (two-colour QCD) at non-zero quark chemical potential was recently presented by Hands *et al.* in Ref. [31]. In contrast to QCD with three colours, in QC$_2$D, the addition of a quark chemical potential does not result in a complex action and numerical calculations can be performed efficiently [32–34]. In Ref. [6] it was pointed out that the phase structure of QCD at nonzero μ_I has an intriguing similarity to that of QC$_2$D at nonzero quark chemical potential. It is apparent that the similarities persist to the case of quarkonium energy shifts in medium as an at least qualitatively similar dependence on the charge density/chemical potential is observed in the two-colour QCD case. Recent work [35–37] has probed the connections between different gauge theories with nonzero (isospin) chemical potentials and, as the extent of this similarity is surprising, this warrants further investigation.

Finally, by looking at quarkonium–pion correlation functions on three different volumes, we have extracted η_b–π and Υ–π scattering phase shifts at low momentum, albeit with significant uncertainties. The interactions are found to be weak in both cases as expected from chiral dynamics.
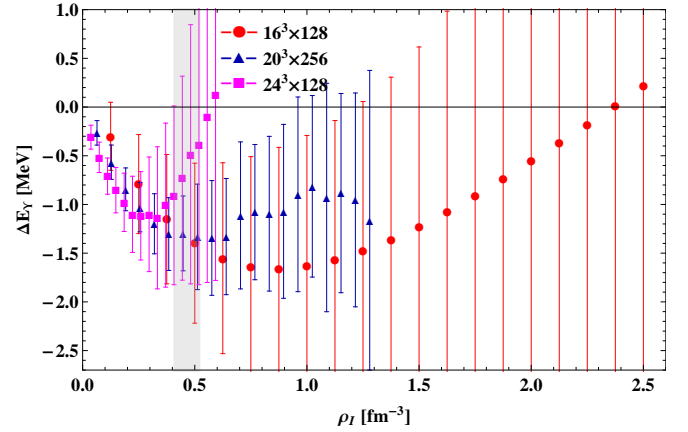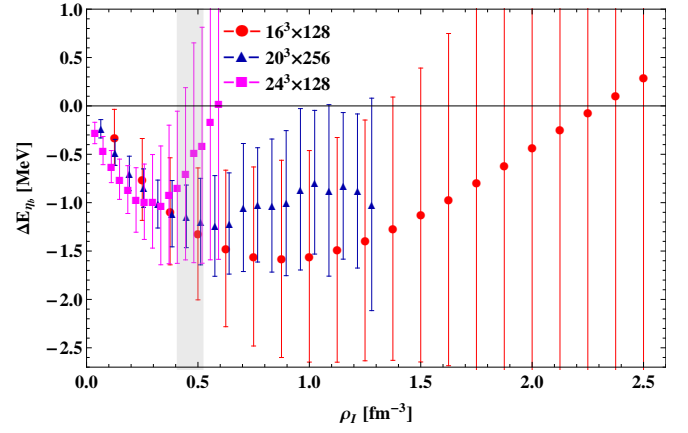
Acknowledgments

FIG. 10: The dependence of the energy shift on the isospin charge density is shown for the three lattice volumes for the η_b (upper panel) and Υ (lower panel). The shaded vertical band in each plot shows the region where there is a peak in the ratio of the pionic energy density to the Stefan-Boltzmann expectation (see Fig. 22 of Ref. [6]).
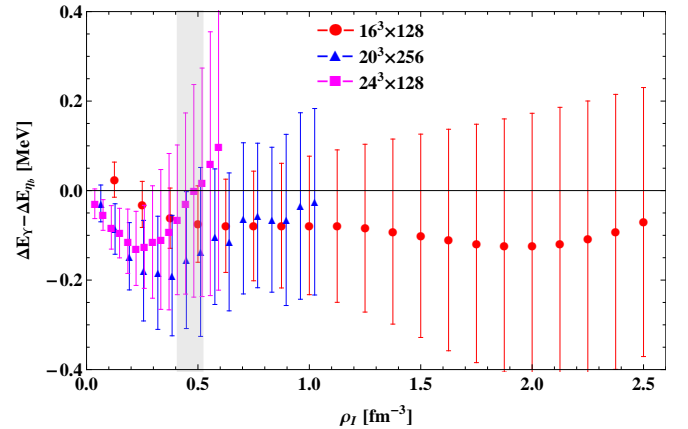

FIG. 11: Isospin density dependence of the shift of the S-wave hyperfine splitting between the Υ and η_b states in medium.
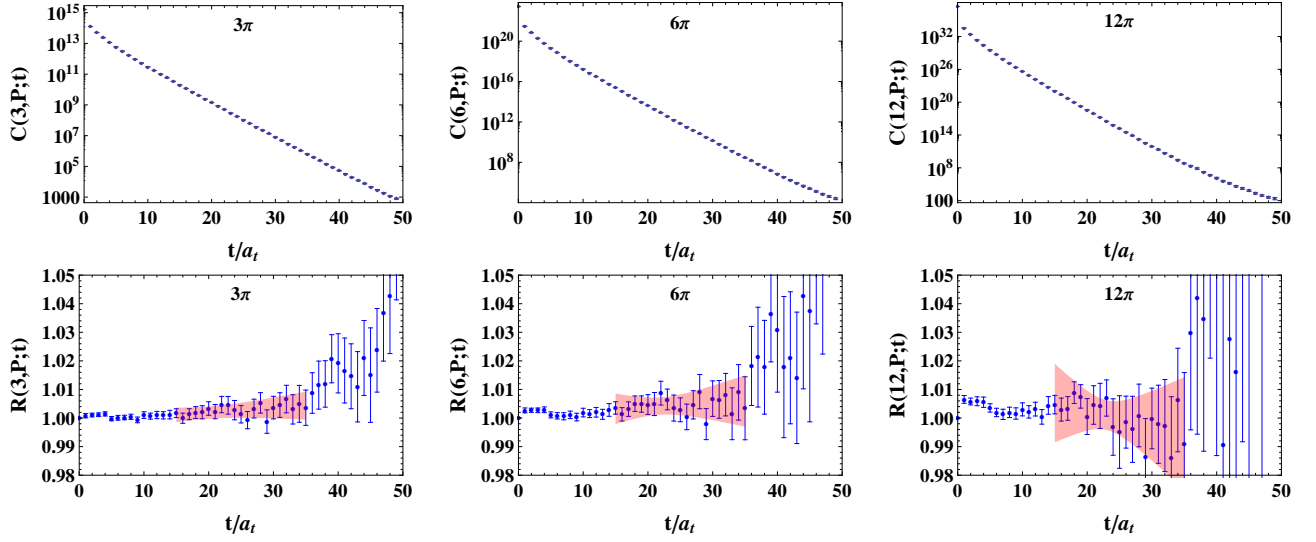
FIG. 12: The correlators (upper) and correlator ratios (lower) corresponding to the spin-averaged P-wave energy in a medium corresponding to isospin charges $n = 3$, 6, and 12, for the $16^3 \times 128$ ensemble.
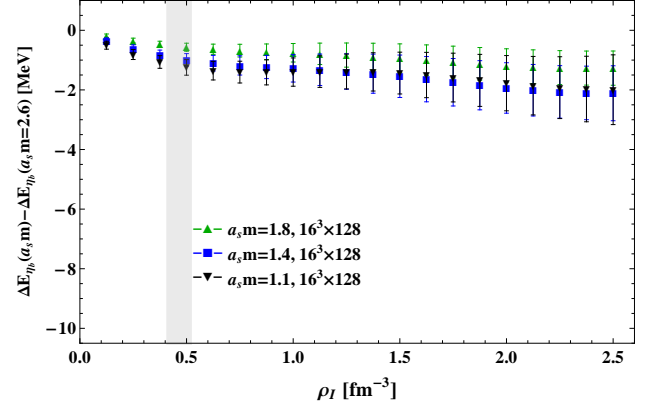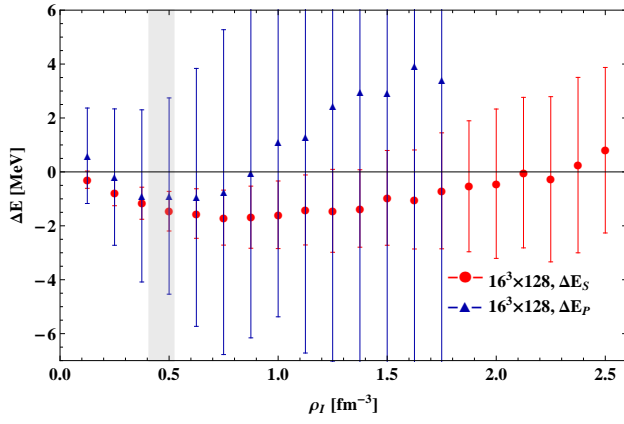

FIG. 13: The extracted energy shift of the spin averaged P-wave quarkonium state as a function of the isospin charge density. Also shown for comparison is the equivalent spin averaged S-wave energy shift and the vertical band shows the isospin density at which the pionic energy density is peaked relative to the Stefan-Boltzmann expectation. Data are shown for the $16^3 \times 128$ ensemble.
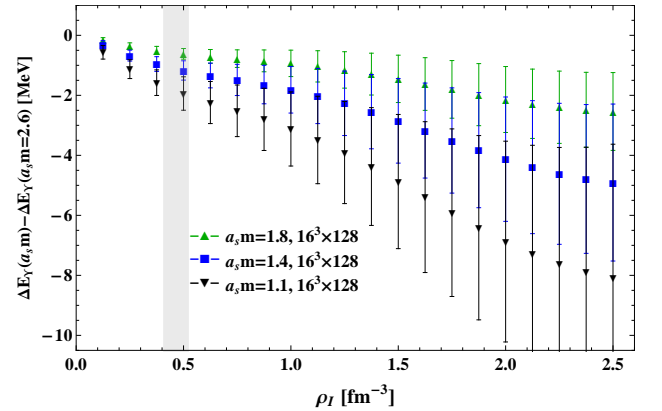
FIG. 14: The difference of the η_b (upper) and Υ (lower) energy shift for a given heavy quark mass from the shift for $a_s m = 2.6$ is shown as a function of the isospin charge density. Results are shown for the $16^3 \times 128$ ensemble.

n	$\Delta E_{n;\Upsilon}$			$\Delta E_{n;\eta_b}$		
	$16^3 \times 128$	$20^3 \times 256$	$24^3 \times 128$	$16^3 \times 128$	$20^3 \times 256$	$24^3 \times 128$
1	$-0.32(15)(25)$	$-0.24(09)(04)$	$-0.28(10)(04)$	$-0.30(17)(31)$	$-0.26(11)(05)$	$-0.31(12)(01)$
2	$-0.76(21)(37)$	$-0.48(12)(06)$	$-0.46(14)(05)$	$-0.79(23)(45)$	$-0.57(16)(07)$	$-0.52(15)(03)$
3	$-1.09(29)(47)$	$-0.70(16)(07)$	$-0.63(15)(07)$	$-1.15(32)(58)$	$-0.84(20)(09)$	$-0.71(18)(05)$
4	$-1.32(37)(57)$	$-0.85(18)(08)$	$-0.76(20)(07)$	$-1.40(41)(71)$	$-1.03(23)(10)$	$-0.85(23)(06)$
5	$-1.47(46)(66)$	$-1.01(24)(08)$	$-0.86(24)(05)$	$-1.55(51)(84)$	$-1.20(30)(08)$	$-0.98(29)(06)$
6	$-1.56(56)(74)$	$-1.11(34)(07)$	$-0.97(33)(05)$	$-1.64(62)(94)$	$-1.30(37)(07)$	$-1.10(39)(06)$
7	$-1.58(66)(77)$	$-1.14(32)(06)$	$-0.99(38)(09)$	$-1.7(0.7)(1.0)$	$-1.30(38)(05)$	$-1.12(45)(08)$
8	$-1.55(77)(78)$	$-1.20(44)(06)$	$-0.99(47)(13)$	$-1.6(0.8)(1.0)$	$-1.33(54)(05)$	$-1.10(57)(13)$
9	$-1.49(88)(76)$	$-1.24(52)(05)$	$-1.03(58)(21)$	$-1.5(1.0)(1.1)$	$-1.34(59)(06)$	$-1.14(71)(17)$
10	$-1.4(1.0)(0.7)$	$-1.22(52)(05)$	$-0.92(65)(29)$	$-1.5(1.1)(1.1)$	$-1.33(59)(07)$	$-1.01(80)(26)$
11	$-1.3(1.1)(0.7)$	$-1.05(66)(07)$	$-0.84(72)(31)$	$-1.4(1.3)(1.1)$	$-1.11(75)(10)$	$-0.91(87)(30)$
12	$-1.1(1.3)(0.8)$	$-1.02(59)(07)$	$-0.70(78)(43)$	$-1.2(1.4)(1.1)$	$-1.08(69)(11)$	$-0.73(96)(43)$
13	$-1.0(1.5)(0.8)$	$-1.03(68)(09)$	$-0.5(1.0)(0.5)$	$-1.1(1.7)(1.2)$	$-1.10(78)(13)$	$-0.5(1.2)(0.5)$
14	$-0.8(1.7)(0.9)$	$-1.01(74)(11)$	$-0.4(1.1)(0.6)$	$-0.9(1.9)(1.3)$	$-1.07(88)(17)$	$-0.4(1.3)(0.6)$
15	$-0.6(1.9)(1.0)$	$-0.86(83)(10)$	$-0.2(1.3)(0.7)$	$-0.7(2.1)(1.5)$	$-0.90(99)(16)$	$-0.1(1.5)(0.8)$
16	$-0.4(2.1)(1.2)$	$-0.79(73)(14)$	$0.0(1.4)(0.8)$	$-0.6(2.3)(1.6)$	$-0.81(90)(23)$	$0.1(1.7)(0.9)$
17	$-0.3(2.3)(1.3)$	$-0.87(87)(15)$	$0.0(1.6)(0.8)$	$-0.4(2.5)(1.7)$	$-0.9(1.1)(0.3)$	$0.1(1.9)(0.9)$
18	$-0.1(2.5)(1.5)$	$-0.83(73)(19)$	$0.5(1.9)(1.0)$	$-0.2(2.6)(1.9)$	$-0.88(96)(36)$	$0.6(2.3)(1.1)$
19	$0.1(2.6)(1.6)$	$-0.88(77)(20)$	$0.2(1.9)(0.9)$	$0.0(2.8)(2.0)$	$-1.0(1.0)(0.4)$	$0.3(2.2)(1.0)$
20	$0.3(2.7)(1.7)$	$-1.0(1.1)(0.3)$	$0.4(2.0)(1.0)$	$0.2(2.9)(2.1)$	$-1.2(1.4)(0.6)$	$0.6(2.3)(1.1)$

TABLE VI: Fits to the S-wave correlator ratios on the various ensembles for $a_s m = 2.6$. For each combination, we report: the mean and the statistical and systematic uncertainties.

[1] T. Matsui and H. Satz, Phys.Lett. **B178**, 416 (1986).
[2] S. Chatrchyan et al. (CMS Collaboration), Phys.Rev.Lett. **107**, 052302 (2011), 1105.4894.
[3] P. Petreczky, J.Phys. **G39**, 093002 (2012), 1203.5320.
[4] G. Aarts, C. Allton, S. Kim, M. P. Lombardo, M. B. Oktay, et al. (2012), 1210.2903.
[5] W. Detmold and M. J. Savage, Phys.Rev.Lett. **102**, 032004 (2009), 0809.0892.
[6] W. Detmold, K. Orginos, and Z. Shi, Phys.Rev. **D86**, 054507 (2012), 1205.4224.
[7] D. Son and M. A. Stephanov, Phys.Rev.Lett. **86**, 592 (2001), hep-ph/0005225.
[8] A. Hasenfratz and F. Knechtli, Phys.Rev. **D64**, 034504 (2001), hep-lat/0103029.
[9] G. S. Bali, K. Schilling, and A. Wachter, Phys.Rev. **D56**, 2566 (1997), hep-lat/9703019.
[10] R. G. Edwards, B. Joo, and H.-W. Lin, Phys.Rev. **D78**, 054501 (2008), 0803.3960.
[11] H.-W. Lin et al. (Hadron Spectrum Collaboration), Phys.Rev. **D79**, 034502 (2009), 0810.3588.
[12] M. Lüscher and P. Weisz, Commun.Math.Phys. **97**, 59 (1985).
[13] B. Sheikholeslami and R. Wohlert, Nucl.Phys. **B259**, 572 (1985).
[14] C. Morningstar and M. J. Peardon, Phys.Rev. **D69**, 054501 (2004), hep-lat/0311018.
[15] S. R. Beane, W. Detmold, T. C. Luu, K. Orginos, M. J. Savage, et al., Phys.Rev.Lett. **100**, 082004 (2008), 0710.1827.
[16] W. Detmold, M. J. Savage, A. Torok, S. R. Beane, T. C. Luu, et al., Phys.Rev. **D78**, 014507 (2008), 0803.2728.
[17] W. Detmold, K. Orginos, M. J. Savage, and A. Walker-Loud, Phys.Rev. **D78**, 054514 (2008), 0807.1856.
[18] W. Detmold and M. J. Savage, Phys.Rev. **D82**, 014511 (2010), 1001.2768.
[19] W. Detmold and B. Smigielski, Phys.Rev. **D84**, 014508 (2011), 1103.4362.
[20] B. Thacker and G. P. Lepage, Phys.Rev. **D43**, 196 (1991).
[21] G. P. Lepage, L. Magnea, C. Nakhleh, U. Magnea, and K. Hornbostel, Phys.Rev. **D46**, 4052 (1992), hep-lat/9205007.
[22] I. Drummond, R. Horgan, T. Manke, and H. Shanahan, Nucl.Phys.Proc.Suppl. **73**, 336 (1999), hep-lat/9809170.
[23] T. Manke et al. (CP-PACS Collaboration), Phys.Rev.Lett. **82**, 4396 (1999), hep-lat/9812017.
[24] I. Drummond, N. Goodman, R. Horgan, H. Shanahan, and L. Storoni, Phys.Lett. **B478**, 151 (2000), hep-lat/9912041.
[25] G. Aarts, C. Allton, S. Kim, M. Lombardo, M. Oktay, et al., JHEP **1111**, 103 (2011), 1109.4496.
[26] S. Meinel, Phys.Rev. **D82**, 114502 (2010), 1007.3966.
[27] G. P. Lepage and P. B. Mackenzie, Phys.Rev. **D48**, 2250 (1993), hep-lat/9209022.
[28] M. Lüscher, Commun.Math.Phys. **105**, 153 (1986).
[29] M. Lüscher, Nucl.Phys. **B354**, 531 (1991).
[30] S. R. Beane, P. F. Bedaque, T. C. Luu, K. Orginos, E. Pallante, et al., Phys.Rev. **D74**, 114503 (2006), hep-lat/0607036.
[31] S. Hands, S. Kim, and J.-I. Skullerud, Phys.Lett. **B711**, 199 (2012), 1202.4353.
[32] S. Hands, S. Kim, and J.-I. Skullerud, Eur.Phys.J. **C48**, 193 (2006), hep-lat/0604004.
[33] S. Hands, P. Sitch, and J.-I. Skullerud, Phys.Lett. **B662**, 405 (2008), 0710.1966.
[34] S. Hands, S. Kim, and J.-I. Skullerud, Phys.Rev. **D81**, 091502 (2010), 1001.1682.
[35] A. Cherman and B. C. Tiburzi, JHEP **1106**, 034 (2011), 1103.1639.
[36] M. Hanada and N. Yamamoto, JHEP **1202**, 138 (2012), 1103.5480.
[37] M. Hanada, C. Hoyos, A. Karch, and L. G. Yaffe, JHEP **1208**, 081 (2012), 1201.3718.
[38] R. G. Edwards and B. Joo (SciDAC Collaboration, LHPC Collaboration, UKQCD Collaboration), Nucl.Phys.Proc.Suppl. **140**, 832 (2005), hep-lat/0409003.